JJEES

JJEES (2023) 14 (1): 75-82
ISSN 1995-6681

Jordan Journal of Earth and Environmental Sciences

Kinematic Analysis of Amman-Hallabat Structure, Northeast Dead Sea, Jordan

Masdouq Al-Taj

Department of Earth Sciences and Environment, Prince El Hassan Bin Talal Faculty for Natural Resources and Environment, The Hashemite University, P.O. Box 330127, Zarqa 13133, Jordan.

Received 4th April 2022; Accepted 3rd July 2022

Abstract

In this study, a new collection of kinematic data sets relating to the Amman-Hallabat Structure (AHS) is presented. Measurements of fault slip were taken over the near field of a structure that was thirty kilometers long and located northeast of the Dead Sea. The kinematic study that was carried out as a consequence reveals that strike-slip faulting predominates, along with minor episodes of oblique-slip and reverse faulting. Overall, there is a regional coherence in the orientations of the extensional and shortening axes associated with both types of faulting over the whole research area. This coherence can be seen in the orientations of the extensional and shortening axes. It is suggested that the data set be interpreted as the result of sinistrally transpressive kinematics that are more or less continuous, with shortening axes mainly oriented NW–SE to NNW–SSE and minor NE-SW and extensional axes predominately oriented NE–SW and minor NW–SE. These kinematic axes result from the two stress fields that affect the area, the earlier Syrian Arc Stress and the later Dead Sea Stress. The multistage kinematic history of the AHS indicates that the stress fields that generates AHS are kinematically incompatible.

Keywords: *Kinematic analysis, Amman-Hallabat Structure, Dead Sea Transform, Syrian Arc, Strain axis.*

1. Introduction

The development of the Syrian Arc Fold System (SAFS) in the Upper Cretaceous and the movement of the Arabian Plate in the Miocene-Recent define the structural deformation of Jordan (Abed, 2017). The Syrian Arc Fold System is an "S" shape and consists of a sequence of asymmetric anticlines and synclines that extend from Egypt's Sinai Peninsula to the Palmyrides in Syria (Fig. 1) (Moustafa, 2013). The general trend of the whole folded belt varies from NE (Sinai and Naqab) to NNE (central part) and then back to NE (Palmyrides in Syria). The entire SAFS started folding in the late Turonian when the early Mesozoic extensional stress field changed to a compressional stress field with maximum shortening oriented WNW-ESE. (Eyal, 2011; Guiraud and Bosworth, 1997).

The Dead Sea Transform Fault (DST) is 1100 km long and separates the Arabian and Sinai-Palestine plates (Fig. 2) (Lu et al., 2020; Hempton, 1987; Garfunkel, 1981). It accommodated about 105 km of left-lateral displacement (Garfunkel, 1981; Freund et al., 1970; Quennell, 1958). The DST connects the Gulf of Aqaba in the south with the Karasu Valley in southeast Turkey in the north (Mahmoud et al., 2012). Several Pliocene-Quaternary basins are conjoined as the Dead Sea Basin and the Ghab Basin (Brew et al., 2001). The beginning age of the DST is the Early Miocene (Freund et al., 1970), or the Early-Middle Miocene with increasing displacement in the Pliocene-Quaternary (Steckler and Ten Brink, 1986). Several regional models estimated relative motion along the DST at 5 to 10 mm/yr (Meghraoui, 2015; Ferry et al., 2011; Chu and Gordon, 1998; Joffe and Garfunkel, 1987; Garfunkel, 1981). According to space geodetic techniques, the current slip rate across the DST is 4.9 + 0.4 mm/yr (Hamiel et al., 2018; Al Tarazi et al., 2011). The maximum horizontal axis of compression near the DST is NNW-SSE (e.g., Diabat, 2009; Zain Eldeen et al., 2002) (Fig. 2). Many inherited structures, such as the Syrian Arc, accommodate this stress (Alchalbi et al., 2010; Abou Romieh et al., 2009; Badawy and Horváth, 1999; Chaimov et al., 1990). The southern part of the DST has two structures; the Wadi Araba Fault (WAF) and the Jordan Valley Fault (JVF) (Fig. 2) (i.e Beon et al., 2010; Ferry et al., 2007). The WAF, with 250 km in length, is a sinistral strike-slip fault composed of several segments connected by either small-scale thrust edges or pull-apart basins (Ferry et al., 2011; Le Beon et al., 2010, 2008; Hofstetter et al., 2007; Klinger et al., 2000; Atallah, 1992; Garfunkel, 1981). At the northeast corner of the Dead Sea, WAF shows a change in direction to the northeast, forming a restraining bend with the sinistral sense of movement and merging with two geological structures: the Amman Hallabat Structure (AHS) and the Shueib Structure (SHS) (Fig. 1) (Al Hseinat et al., 2020; Mikbel and Zacher, 1981). The two structures were formed in an NW-SE compressive framework, producing NE-SW folds and reverse faults in the upper Cretaceous and superimposed on the Syrian Arc (Al-Awabdeh et al., 2016; Diabat, 2009).

* Corresponding author e-mail: maltaj@hu.edu.jo

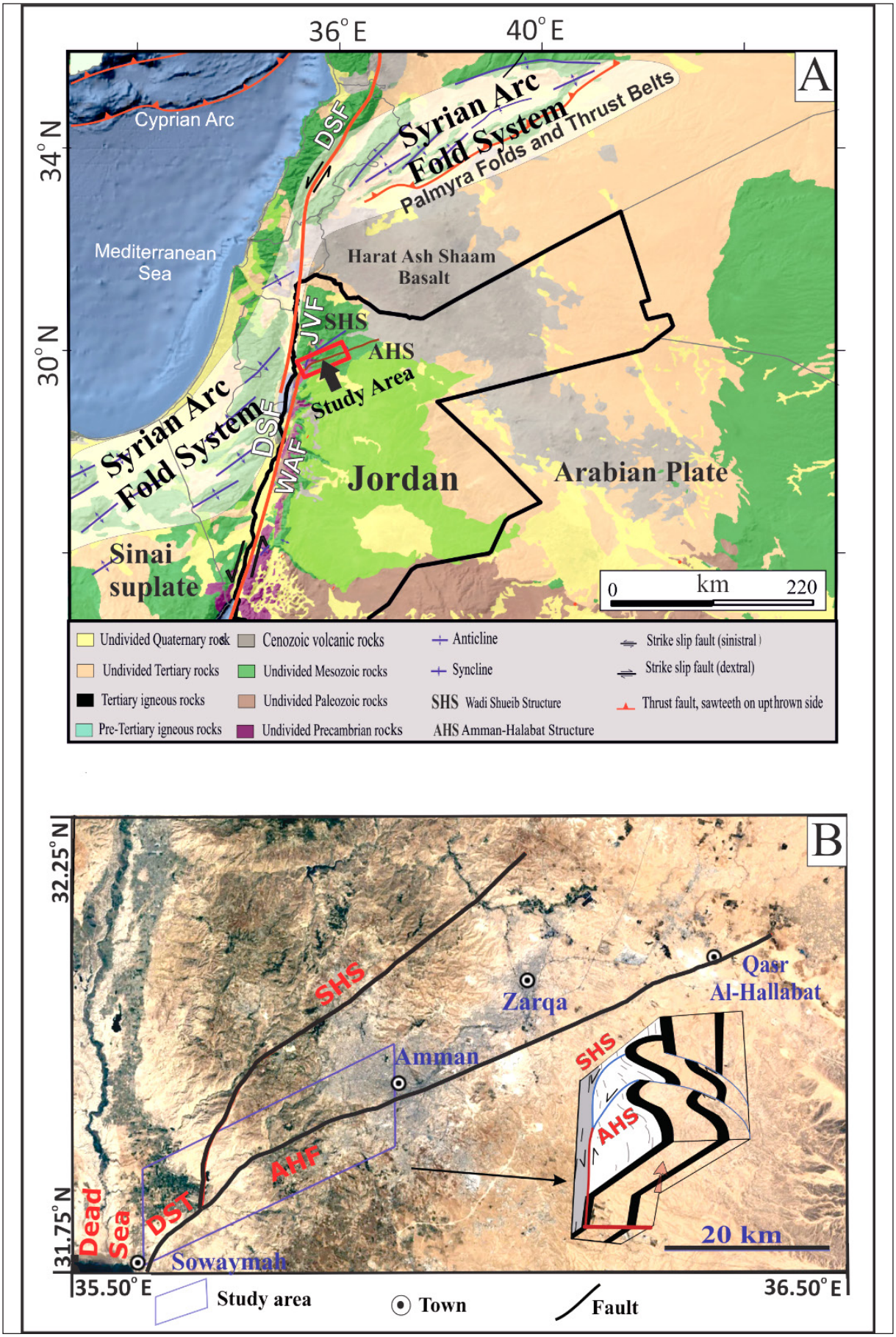

Figure 1. The Syrian Arc fold system and main structures in Jordan (A). The inset shows the location of the study area, (B) Amman -Hallabat Fault (AHF), Shuaib Structure (SHS), and a simplified model shows 3D of AHS and SHS (Modified from Al Hseinat et al., 2020).

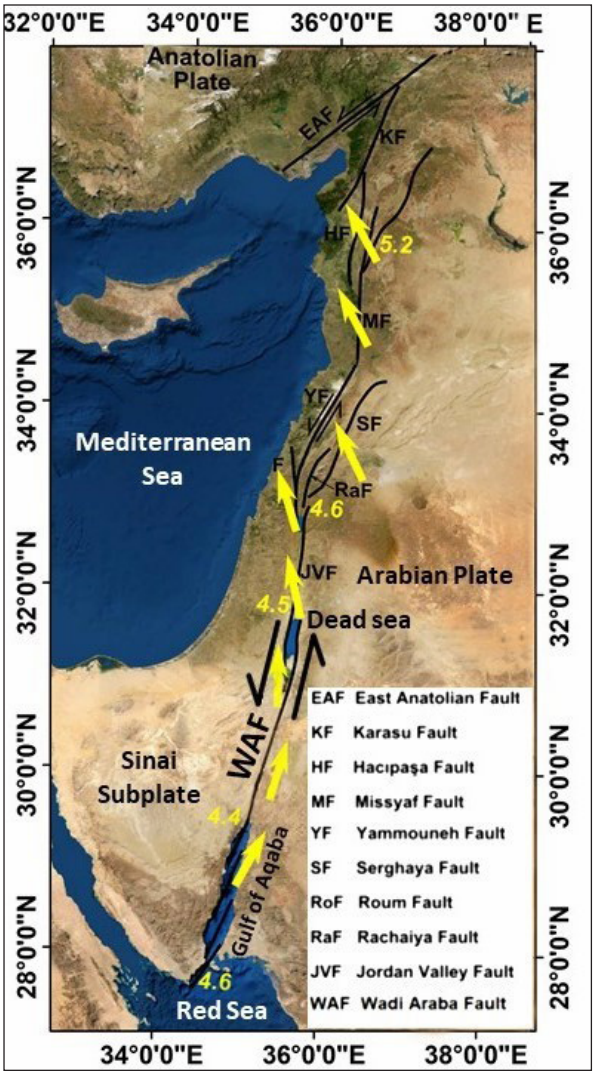

Figure 2. Dead Sea Transform fault (DST). Yellow arrows and numbers show the direction and amount of movement of the Arabian Plate concerning the Africa Plate in mm per year (Modified from Gomez et al., 2007).

2. Geological Setting

2. 1 Stratigraphy of the area

The Triassic Zarqa Ma'in Group is the oldest rock unit in the study area (Fig. 3). It is composed mainly of sandstone, sandy limestone, and dolomite (Makhlouf, 2003). The Azab Jurassic Group was sub-divided into 7 formations (Abed, 2017; Andrews, 1992): Hihi claystone, Nimir limestone, Silal sandstone, Dahab limestone, Ramla sandstone, Hamam sandstone, and Mughanyya limestone. The early Cretaceous, Kurnub Sandstone Group, overlies unconformably Triassic and Jurassic sediments in the southern and northern areas, respectively. It consists of braided-rivers sand deposits (Andrews, 1992). The late Cretaceous to the early Paleogene, Ajlun, and Belqa groups, consist predominantly of limestone, chalk, marls, chert, and phosphate. Ajlun Group was divided into five formations; they are from older to younger: Na'ur, Fuhies, Hummar, Shueib, and Wadi As Sir formations (Masri, 1963; Powell, 1989; Abed, 2017). Whereas Belqa Group was divided into five formations, they are from older to younger: Wadi Umm Ghudran, Amman Silicified, Al Hisa Phosphorite, Muwaqqar Chalk-Marl and Umm Rijam Chert-Limestone formations (Powell, 1989). The lower three formations are exposed in the study area whereas the upper two formations are exposed to the east of the area. The Neogene is largely eroded; Lisan and Damya formations represent the late Quaternary sediments in the study area (Fig. 3).

2.2 Tectonic setting of the area

According to Bender (1968), the study area is located within the highlands east of the DST and the Amman plateau (East Jordanian Plateau). Two main structures represent the Syrian arc in Jordan: The AHS is about 80 km long and extends from WAF in the west to Qasr Al Hallabat in the east of Jordan (Fig. 1) (Al Hseinat et al., 2020; Diabat, 2009; Mikbel and Zacher, 1981). The SHS represents a NE-SW oblique reverse fault with sub-parallel folds. This Structure was active in the late Cretaceous period. The study of Al-Awabdeh et al., (2016) proposed a Neogene reactivation of local faults in this structure as linked to the transpression activity of the DST. AHF is a NE–SW to ENE–WSW strike-slip fault and sub-parallel to anticlines and synclines (Mikbel and Zacher, 1986). In the eastern part of the studied area, the Amman Formation (Santonian-Campanian) on the northwestern side of the AHS is downfaulted against Wadi As Sir Formation (Turonian) on the southeastern side of the AHS. The downthrow of this fault is in the NNW direction (Diabat, 2009). Both the late Cretaceous (AHF and faults of SHS) are associated with ESE-WNW maximum compressive stress. Those structures were inactive during the Neogene (Sahawneh and Atallah, 2002; Mikbel and Zacher, 1981). Diabat (2009) proposed that they have a Quaternary activity and showed a significant similarity between the stress field orientation related to the DST. Recently, Al Hseinat et al. (2020) supposed that the DSF has combined with the main faults of the AHS. They further supposed that these faults were reactivated as a restraining bend formed from the DSF branches that developed due to the NNW-SSE-trending Dead Sea transpressional stress field. Thrust components are present on faults with horsetail geometry depending on the interaction between the direction of the AHS strands and the regional tectonic displacement along the DST. These movements are followed by folding and uplifting. Consequently, the main faults in the AHS have a horsetail structure, with folds and thrusting deformation.

3. Methodology

The current research focused on the kinematics of the AHS, where the structures are spatially continuous and bound by the DST and SHS (Fig. 1). Seven stations (S1-S7) were selected to perform the required measurements over a 30-kilometer length between the WAF in the west and the Amman area in the east (Fig. 3). The majority of the measurements were taken at Cretaceous outcrops. The study focuses on carbonate rocks that indicate reliable lineations or growth fibers on the fault planes. Due to the nature of the outcrop in the region, a relatively small number of observations were collected. All data acquired for this investigation consist of fault plane-striation pair measurements. The sense of movement on the plane was

determined by shear sense indicators, namely striations, and fibers on fault planes, which were observed to be highly developed in carbonate rocks (Fig. 4). To eliminate bias in the data set, one measurement per fault plane-striation was acquired, and only fault planes exhibiting shear indicators have been included in the kinematic analysis. To justify the relatively small set of data we have gathered, it is important to note that the fault-slip data from the quarries analyzed in this study are the only coherent data sets identified in the carbonate strata of the investigated sites.

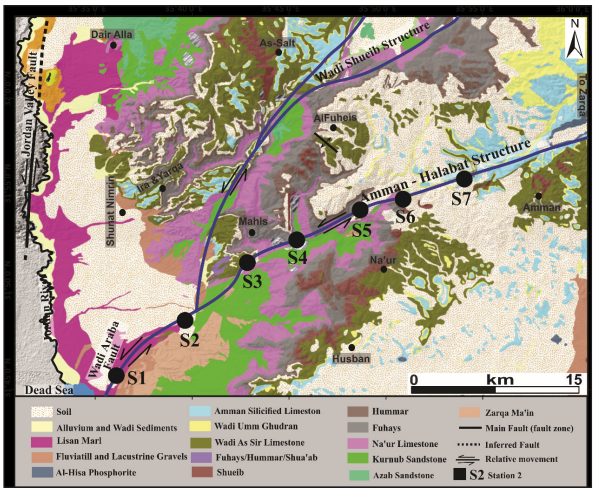

Figure 3. Geological Map and Locations of the measurement stations. The stations are marked by black circles and numbered from S1 to S7. (Geological map modified from Al Hseinat et al., 2020).

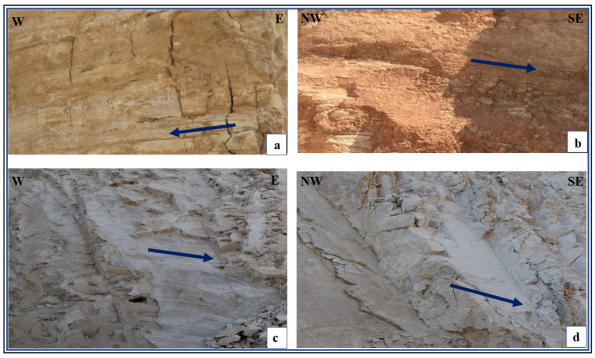

Figure 4. Fault-plane kinematic indicators. (a) Slickenlines on dextral strike-slip fault. (b) grooves on oblique-slip fault. (c) and (d) calcite mineral growth fiber on sinistral strike-slip faults. In (a) and (b) the arrow indicates the movement of the lost wall.

The Multiple Slip Method (MSM) (Zalohar and Vrabec, 2008) was used to calculate the common extension, intermediate, and shortening axes of a population of fault slip data. The MSM is an updated and modified version of the moment tensor summation (MTS) method developed by Kostrov (1974), Molnar (1983), and Marrett and Allmendinger (1991, 1990) and the finite strain and rotation from the fault slip method of Cladouhos and Allmendinger (1993). The MSM method is based on the theory of Linear Elastic Fracture Mechanics (LEFM) and the theory of scaling of fracture and fault systems. The main goal of the MSM method is to give an alternative way to figure out the weighting factors in the infinitesimal method of summing the moment tensor.

In general, the MSM method allows for calculating the macro-strain and relative micro-rotation tensors. This method allows constraining the fields P (shortening axis) and T (extension axis) delimited by each fault. The vectors of this tensor are parallel to the kinematic axes P, B (middle axis), and T of the fault. In this case, each fault's P and T fields are approximately similar to the corresponding fields (P and T) defined by the common macro-strain tensor. The axes determined for extension and shortening were examined for agreement with the results obtained using the P-T axes method (Jena and Pradhan, 2020). T-Tecto Studio X5 software (Zalohar, 2020) was used to perform the MSM method calculations.

4. Results of kinematic analysis

The number of fault-slip field measurements is 91 (Figs. 5 and 6), but the data used in the analysis is 77 (Fig. 7); the 14 field measurements were discarded since they are incompatible with slip deviations and provide inaccurate results. So. This research was confined to planes having reliable shear indicators, resulting in a somewhat small but significant data set. Measurements were taken at quarries near the AHS. The NE-SW oriented major direction of all fault planes, as shown in the rose diagram at the top of Fig. 6, agrees with AHS. This direction is well presented in the rose diagram of all reverse faults measured in the stations (Fig. 5c and Fig. 6) and less illustrated in the rose diagram of dextral and sinistral strike-slip faults measured in the stations (Figs. 5a and b). The strike-slip faults are sub-verticals with striations pitched between 0° and more than 30° (Fig. 6). The large values of striations pitch are due to later deformation episodes. The dextral and sinistral faults are largely similar in directions (Figs. 5a and b) which suggest the existence of many compressive episodes, with NW-SE and NE-SW shortening axes or faults reactivation, or strength anisotropy, providing cause for the generation of the dextral and sinistral faults.

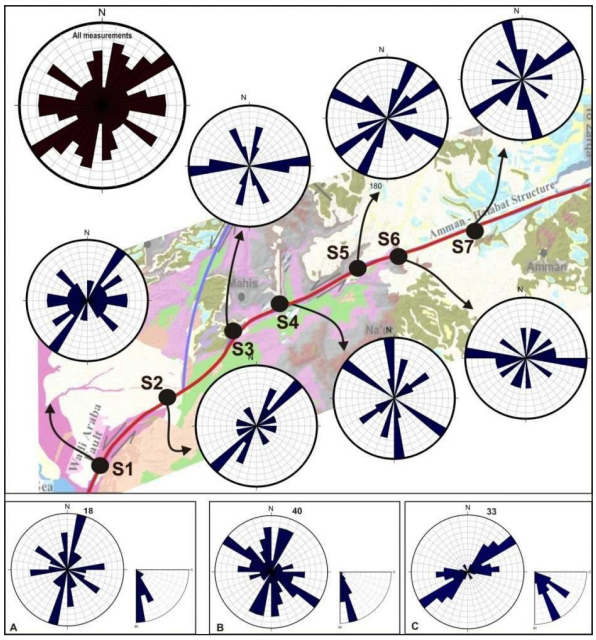

Figure 5. Fault geometries: Rose diagram of fault orientations measured at every station.

Rose diagram of all: a-Dextral strike-slip, b- Sinistral strike-slip, and c- Reverse faults measured in the whole stations. The Rose diagram at the top of the figure presents the direction of all fault types in all stations. (Base map from Al Hseinat et al. 2020)).

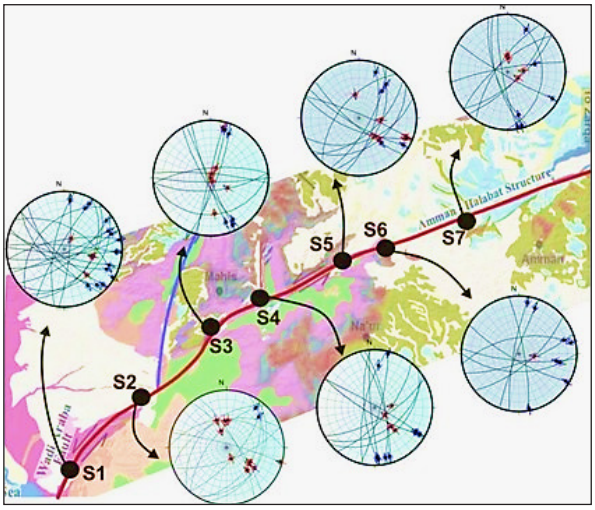

Figure 6. Lower hemisphere projections show measured fault plane-striation for each station. Red points with arrowheads on striation plunge symbols indicate the sense of displacement of hanging wall blocks of reverse faults, and blue points with arrows indicate the sense of displacement on strike-slip faults. (Base map from Al Hseinat et al., 2020).).

The MSM method was applied to the obtained station data. Results are documented in Table 1 and shown in Fig. 7. The best-determined solutions were obtained from those sites where the measurements were divided into fault sets (S1, S2, S4, and S5). However, some sites with few data measurements (S3, S6, and S7) also give reasonable results. The majority of the sites have strike-slip solutions with axes of shortening in the NW–SE to NNW–SSE and the NE–SW orientations (Fig. 7). Reverse faults present an NNW–SSE shortening direction of some of the sites (S2 and S5, Fig. 7). Rotation along the faults is likely to be caused by the tilting of the beds at some locations. The oblique-slip solutions at several sites demonstrate the deviations from kinematic calculations. Normal faulting was not obtained in the studied area.

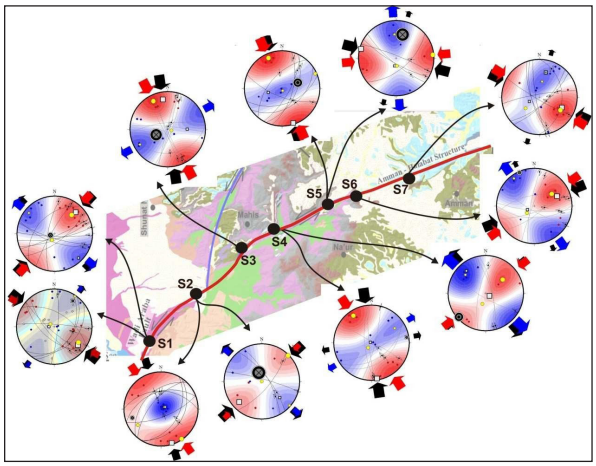

Figure 7. P- and T-axes for the measured faults as calculated by using the MSM method. Mean orientations for the P (horizontal shortening=red arrow), T (horizontal extension=blue arrow), and rotation axes (black arrows). The coinciding of black arrows and Kinematic axes means pure shear. Otherwise, it means simple shear and strain axes rotation with incremental strain. (Base map from Al Hseinat et al., 2020).

The positions of the calculated shortening axes are horizontal or close to horizontal (Fig. 8). Analyzing kinematic measurements present several shortening axes trends within the AHS. The main direction of the shortening axis is presented in the rose diagram attached at the top of Fig. 8. The dominant direction is NNW-SSE to NW-SE. The less important direction of shortening is NE-SW. Analyzing both reverse and strike-slip faults present NNW-SSE to NW-SE direction of shortening, whereas the NE-SW direction is a result of only strike-slip fault analysis.

Table 1. Results of kinematic analysis (trend and plunge) of the principal axes of strain obtained from SMS calculations. N: number of fault measurements.

Location and Number		Axis 1		Axis 2	Axis 3	
Station	N	Shortening		Intermediate	Extension	
S1 -a	9	123/14	(NW-SE)	304/76	035/0	(NE-SW)
S1 -b	10	042/21	(NE-SW)	204/68	309/6	(NW-SE)
S2 -a	7	145/0	(NW-SE)	235/14	065/76	(NE-SW)
S2 -b	4	046/0	(NE-SW)	304/90	131/0	(NW-SE)
S3	9	333/9	(NNW-SSE)	109/77	241/9	(NE-SW)
S4 -a	7	326/7	(NW-SE)	213/72	058/17	(NE-SW)
S4 -b	4	051/29	(NE-SW)	196/56	312/17	(NW-SE)
S5 -a	7	336/6	(NW-SE)	066/1	162/83	(NNW-SSE)
S5 -b	4	085/0	(E-W)	175/66	356/24	(N-S)
S6	8	055/30	(NE-SW)	226/59	323/4	(NW-SE)
S7	8	122/22	(NW-SE)	231/38	010/44	(NNE-SSW)

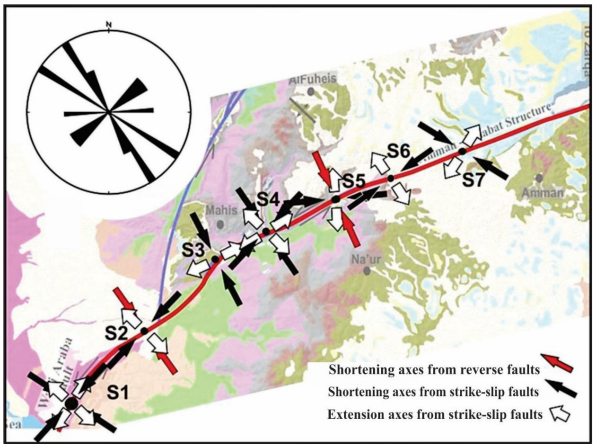

Figure 8. Shortening (black and red) and stretching axes (white) from MSM calculations in the AHS (Table 1). The Rose diagram at the top of the figure presents the main directions of the shortening axes for all stations. (Base map from Al Hseinat et al., 2020).

5. Discussion

The geometry of the measured fault in the different stations along the AHS should already be a reflection of its kinematics. Then, we have to agree that the AHS must have originated as a reverse fault with an important strike-slip component and has been found in this manner since its formation, and it has developed in different stages (Al-Awabdeh et al., 2016; Diabat, 2009). Zoback (1992) showed that mechanical anisotropies at a large-scale fault zone could modify the stress axes' orientation. Therefore, the origin of principal strain deviation from fault populations of known kinematics mustn't be considered problematic. The MSM method shows a combined NW–SE and NE–SW shortening axes and NE–SW stretching axes with local deviations (Fig. 8). Most of the shear indicators measured in the stations agree with this kinematics (Fig. 4). The kinematic structures in the studied area are strike-slip and reverse movements. Strike-slip and dip-slip kinematic indicators on the fault planes suggest that the faults were reactivated later.

The AHS accommodates the NE–SW trending reverse faults and the NE–SW faults with sinistral movement. These latter fault trends are due to the inherited structure of the Syrian Arc in the AHS which resulted from the E-W to ENE-WSW stress field. These transpressive structures are probably operated since the upper Cretaceous. The Senonian shortening in the western Syrian Arc was NNW-SSE directed and changed progressively to NW-SE and nearly WNW-ESE in Palestine (Sehim, 1993; Letouzey and Tremolibres, 1980). However, the cause of these transpressive structures may be a local response to anticlockwise rotation of the horizontal NNW–SSE shortening at restraining bends near WAF and AHS (Al-Taj et al., 2007).

The calculated kinematic axes correspond to many phases of tectonic development that control the AHS's deformations (Fig. 8). The geometry of the reverse faults measured in the AHS and adjoining NE-SW folds agrees with the NW-SE shortening axis. The NNW-SSE shortening axis accommodated the DST deformation and affected the geometry of the AHS at a later stage of its initial formation. It is suggested that the strain field of the NNW-SSE shortening axes in the AHS zone is consistent with sinistral movement on the fault. The NW-SE shortening field related to sinistral strike-slip faults is presented in the studied area (Fig. 8). As has been shown in previous works (Al Hseinat et al., 2020; Eyal and Eyal, 2015; Hofstetter et al., 2007; Badawy and Horváth, 1999; Eyal, 1996; Chaimov et al., 1990), it agrees with the present-day kinematics field of the DST. The results of kinematic axes indicate that the Dead Sea stress and the Syrian Arc Stress fields are kinematically incompatible.

The acquired observations in the area are in agreement with a change in the strain field of the AHS from thrust deformation during the Cretaceous to strike-slip and oblique reverse faulting in the Neogene. Diabat (2009) proposed a possible Quaternary reactivation in the northernmost part of AHS.

The stress field based on seismological studies (Palano et al., 2013; Hofstetter et al., 2007) showed sinistral movement that drives the deformation in the DST. It is compatible with strain tensors with the NNW–SSE shortening axis. It is suggested that NNW–SSE shortening drives the Quaternary reactivation tectonics in AHS.

6. Conclusions

For the AHS, a small but reliable set of fault slip data has been acquired. Almost all data can be explained by oblique strike-slip and reverse movement dominating the majority of the investigated stations near the AHS. With the notable exception of an extension in the NW–SE direction, there is remarkable coherence in the orientation of the NE–SW extension along the investigated strike length of the AHS. The majority of calculated shortening axes have subhorizontal NW–SE to NW–SE orientations. The kinematic axes indicate that the E-W compressional Syrian Arc stress field and NW-SE Dead Sea stress field with about anticlockwise rotation. The current findings indicate that AHS is produced in more or less continuous, sinistrally transpressional kinematics in space and time.

References

Abed, A. (2017). Geology of Jordan, its water and environment. 2nd Edition (In Arabic), Dar Wael, Amman.

Abou Romieh, M., Westaway, R., Doud, M., Radwan, Y., Yasminh, R., Khalil, A., Al-Ashkar, A., Loughlin, S., Arrell, K., Bridgland, D. (2009). Active crustal shortening in NE Syria revealed by deformed terraces of the River Euphrates. Terra Nova 21: 427-437.

Al Hseinat, M., Al-Rawabdeh, A., Al-Zidaneen, M., Ghanem, H., Al-Taj, M., Diabat, A., Jarrar, G., Atallah, M. (2020). New Insights for Understanding the Structural Deformation Style of the Strike-Slip Regime along the Wadi Shueib and Amman-Hallabat Structures in Jordan Basedbased on Remote Sensing Data Analysis. Geosciences 10, 253.

Al Tarazi, E., Abu Rajab, J., Gomez, F., Cochran, W., Jaafar, R., Ferry, M. (2011). GPS measurements of near-field deformation along the southern Dead Sea Fault System. Geochemistry, Geophysics, Geosystems 12(12). Q12021. doi:10.1029/2011GC003736 https://doi.org/10.1029/2011GC003736

Al-Awabdeh, M., Perez-Pena, J., Azanon, J., Booth-Rea, G., Abed, A., Atallah, M., Galve, J. (2016). Quaternary tectonic activity in NW Jordan: Insights for a new model of transpression–transmission along the southern Dead Sea

Transform Fault. Tectonophysics 693: 465-473.

Alchalbi, A., Daoud, M., Gomez, F., McClusky, S., Reilinger, R., Abu Romeyeh, M., Alsouod, A., Yasmin R., Ballani, B., Darawcheh, R., Sbeinati, R., Radwan, Y., Al Masri, R., Bayerly, M., Al Ghazzi, R., Barazangi, M. (2010). Crustal deformation in northwestern Arabica from GPS measurements in Syria: slow slip rate along the northern Dead Sea Fault. Geophys J Int 180:125–135.

Al-Taj, M., Shaqour, F., Atallah, M. (2007). Morphotectonic indices of the Dead Sea transform, Jordan. Geografia Fisica e Dinamica Quaternaria 30(1): 5-12.

Andrews, I. (1992). Permian, Triassic, and Jurassic Lithostratigraphy in the Subsurface of Jordan. Ministry of Energy and Mineral Resources. Amman, Jordan. https://books.google.jo/books?id=_EbrPgAACAAJ

Atallah, M. (1992). Tectonic evolution of northern Wadi Araba, Jordan. Tectonophysics 204:17–26.

Badawy, A., Horváth, F. (1992). The Sinai subplate and tectonic evolution of the northern Red Sea region. J Geodyn 27:433-450.

Bender, F. (1968). Geologie von Jordanien—Beiträge zur Regionalen Geologie der Erde. Gebruder Borntraeger. Stuttgart, Germany.

Brew, G., Lupa, J., Barazangi M., Sawaf, T., Al-Imam, A., Zaza, T. (2001). Structure and tectonic development of the Dead Sea Fault System and Ghab Basin in Syria. Journal of the Geological Society 158: 665-647.

Cardozo, L., Behrmann, J. (2006). Kinematic analysis of the Upper Rhine Graben boundary fault system, Journal of Structural Geology 28: 1028-1039.

Chaimov, T., Barazangi, M., Al-Saad, D., Sawaf, T., Gebran, A. (1990). Crustal shortening in the Palmyride fold belt, Syria, and implication for movement along the Dead Sea Fault system. Tectonics 9(6): 1369-1386.

Chu, D., Gordon, R. (1998). Current plate motions across the Red Sea. Geophys J Int 135: 313–328.

Cladouhos, T., Allmendinger, R. (1993). Finite strain and rotation from fault slip data. Journal of Structural Geology 15: 771-784.

Diabat, A. (2009). Structural and stress analysis based on fault-slip data in the Amman area, Jordan. J Afr Earth Sci 54:155–162.

Eyal Y. (2011). The Syrian Arc Fold system: Age and rate of folding. Geophysical Research 13, EGU2011-7401, EGU General Assembly.

Eyal, Y. (1996). Stress fluctuations along the Dead Sea rift since the Middle Miocene. Tectonics 15: 157-170.

Eyal, Y., Eyal, M. (2015). Nature of slip transfer between strike-slip faults: The Eastern Sinai (Egypt) shear zone, Dead Sea Transform, Journal of Structural Geology 76: 52-60. https://doi.org/10.1016/j.jsg.2015.03.014.

Ferry, M., Meghraoui, M., Abou Karaki, N., Al-Taj, M., Amoush, H., Al-Dhaisat, S., Barjous, M. (2007). A 48-Kyr-long slip rate history for the Jordan Valley segment of the Dead Sea fault. Earth Planet Sci Lett 260: 394-406.

Ferry, M., Meghraoui, M., Abou Karaki, N., Al-Taj, M., and Khalil, L. (2011). Episodic Behavior of the Jordan Valley Section of the Dead Sea Fault Inferred from a 14-ka-Long Integrated Catalog of Large Earthquakes. Seismol. Soc. Am., Bull 101(1): 39-67.

Freund, R., Garfunkel, Z., Zak, I., Goldberg, M., Weissbrod, T., Derin, B. (1970). The shear along the Dead Sea rift. Philosophical Transactions of the Royal Society, London 267:107–130.

Garfunkel, Z. (1981). Internal structure of the Dead Sea leaky transform (rift) in relation to plate kinematics. Tectonophysics 80: 80–108.

Gomez, F., Karam, G., Khawalie, M., McClusky, S., Vernant, P., Reilinger, R., Jaffar, R., Tabet, C., Khair, K., Barazangi, M. (2007). Global positioning system measurements of strain accumulation and slip transfer through the restraining bend along the Dead Sea fault system in Lebanon. Geophys J Int 168:1021–1028.

Guiraud, R., Bosworth, W. (1997). Senonian basin inversion and rejuvenation of rifting in Africa and Arabia: synthesis and implications to plate-scale tectonics. Tectonophysics 282: 39-82.

Hamiel, Y., Piatibratova, O., Mizrahi, Y., Nahmias, Y., Amir Sagy, A. (2018). Crustal Deformation across the Jericho Valley Section of the Dead Sea Fault as Resolved by Detailed Field and Geodetic Observations. Geophysical Research Letters 45 (7): 3043-3050. https://doi.org/10.1002/2018GL077547

Hempton M. R. (1987). Constraints on Arabian plate motion and extensional history of the Red Sea. Tectonics: 687-705.

Hofstetter, R., Klinger, Y., Amrat, A., Rivera, L., Dorbath, L. (2007). Stress tensor and focal mechanisms along the Dead Sea fault and related elements based on seismological data. Tectonophysics 429:165–181.

Jena, R., Pradhan, B. (2020). A model for visual assessment of fault plane solutions and active tectonics analysis using the global centroid moment tensor catalog. Earth Syst Environ 4: 197–211. https://doi.org/10.1007/s41748-019-00142-9

Joffe, S., Garfunkel, Z. (1987). Plate kinematics of the circum Red Sea. A re-evaluation. Tectonophysics 141: 5-22.

Klinger, Y., Avouac, J., Abou Karaki, N., Dorbath, L., Bourles, D., Reyss, J. (2000). Slip- rate on the Dead Sea transform fault in northern Araba valley. Geophys. J. Int 142: 755-768.

Kostrov, V.V. (1974). Seismic moment and energy of earthquakes, and seismic flow of rocks. Physics of Solid Earth 1: 23-40.

Le Beon, M., Klinger, Y., Al-Qaryouti, M., Mériaux, A., Finkel, R., Elias, A., Mayyas, O., Ryerson, F., Tapponnier, P. (2010). Early Holocene and late Pleistocene slip rates of the southern Dead Sea fault determined from 10Be cosmogenic dating of offset alluvial deposits. J Geophys Int 115: B11414.

Le Beon, M., Klinger, Y., Amrat, A., Agnon, A., Dorbath, L., Baer, G., Ruegg, J., Charade, O., Mayyas, O. (2008). Slip rate and locking depth from GPS profiles across the southern Dead Sea transform. J Geophys Res 113: B11403.

Letouzey, J., and Tremolieres, P. (1980). Palaeostress field around the Mediterranean derived from microtectonics: Comparison with plate tectonic data, Rock Mechanics 9: 173–192.

Lu, Y., Wetzler, N., Waldmann, N., Agnon, A., and Marco, S. (2020). A 220,000-Year-Long Continuous Large Earthquake Record on a Slow-Slipping Plate Boundary. Sci. Adv. 6 (48). doi:10.1126/sciadv.aba4170

Mahmoud, Y., Masson, F., Meghraoui, M., Cakir, Z., Alchalbi, A., Yavaoglu,H., Yönlü, O., Daoud, M., Ergintav, S., Inan, S. (2012). Kinematic study at the junction of the East Anatolian fault and the Dead Sea fault from GPS measurements. Journal of Geodynamics 67: 30-39. doi:10.1016/j.jog.2012.05.006

Makhlouf, I. (2003). Fluvial/tidal interaction at the southern Tethyan strandline during Triassic Mukheiris times in central Jordan. J Asian Earth Sci 21:377-385.

Marrett, R., Allmendinger, R. (1990). Kinematic analysis of fault-slip data. Journal of Structural Geology 12: 973-986.

Marrett, R., Allmendinger, R. (1991). Estimates of strain due to brittle faulting: sampling of fault populations. Journal of Structural Geology 13: 735-738.

Masri, M. (1963) Unpublished report on the geology of the

Amman-Zerqa Area. Central Water Authority, Amman, Jordan.

Mikbel, S., Zacher, W. (1981). Fold structures in northern Jordan. Neues Jahrbuch für Geologie und Paläontologie. Monatshefte 4: 248–256.

Mikbel, S., Zacher, W. (1986). The Wadi Shueib Structure in Jordan: Neues Jahrbuch für Geologie und Paläontologie. Monatshefte 9: 571–576.

Molnar, P. (1983). Average regional strain due to slip on numerous faults of different orientations. Journal of Geophysical Research 88: 6430-6432.

Moustafa, A. (2013). Fold-related faults in the Syrian Arc belt of Northern Egypt. Marine and Petroleum Geology 48: 441-454. 10.1016/j.marpetgeo.2013.08.007

Mustapha Meghraoui, M. (2015). Paleoseismic History of the Dead Sea Fault Zone. Encyclopedia of Earthquake Engineering. 10.1007/978-3-642-36197-5_40-1

Palano, M., González P., Fernández, J. (2013). Strain and stress fields along the Gibraltar Orogenic Arc: constraints on active geodynamics. Gondwana Res 23(3):1071–1088. https://doi.org/10.1016/j.gr.2012.05.021

Powell, J.H. (1989). Stratigraphy and sedimentation of the Phanerozoic rocks in Central and South Jordan, Natural Resources Authority, Jordan, Geology Bulletin, No. 11, Part A, Ram & Khreim Groups, 130p., Part B Kurnub, Ajlun & Belqa Groups, 72p.

Quennell, A.M. (1958). The structural and geomorphic evolution of the Dead Sea Rift. Q. J. Geol. Soc 114: 1-24.

Sahawneh, J., Atallah, M. (2002). Tectonic evolution of the north-eastern corner of the Dead Sea, Jordan. Abhath Al Yarmouk 11: 581–598.

Sehim, A. (1993). Cretaceous tectonic in Egypt. Egyptian Journal of Geology, 37(1):335-372.

Steckler, M. S. & Ten Brink, U. S. (1986). Lithospheric strength variations as a control on new plate boundaries: examples from the northern Red Sea region. Earth and Planetary Science Letters 79: 120–132.

Zain Eldeen, U., Delvaux, D., Jacobs, P. (2002). Tectonic evolution in the Wadi Araba Segment of the Dead Sea Rift, Southwest Jordan. EGU Stephan Mueller Spec. Publ. Ser 2: 63–81.

Zalohar J. (2020). T-TECTO Studio X5, Omega Architect Integrated Software for Structural Analysis of Earthquake Focal-Mechanisms and Fault-Slip Data. file:///C:/Users/Admin/Downloads/T-TECTO%20Studio%20X5%20-%20Introductory%20Tutorial.pdf

Žalohar, J., Vrabec, M. (2008). Combined kinematic and paleostress analysis of fault-slip data: The Multiple-slip method. Journal of Structural Geology 30(12): 1603-1613. 10.1016/j. jsg.

Zoback, M. (1992). First- and second-order patterns of stress in the lithosphere: The World Stress Map project, J. Geophys. Res., 97(B8) 11: 703-728. doi:10.1029/92JB00132

المملكة الأردنية الهاشمية

صندوق دعم البحث العلمي

الجامعة الهاشمية

المجلة الأردنية
لعلوم الأرض والبيئة

JJEES

مجلة علمية عالمية محكمة

المجلد (١٤) العدد (١)

http:// jjees.hu.edu.jo/

ISSN 1995-6681